

Digital Multiphase Composites via Additive Manufacturing

Lawrence T. Smith and Robert B. MacCurdy*

Mechanical properties of traditional engineering materials are typically coupled to each other, presenting a challenge to practitioners with multi-dimensional material property requirements. In this work, continuous, independent control over multiple mechanical properties is demonstrated in composite materials realized using additive manufacturing. For the first time, composites additively manufactured from rigid plastic, soft elastomer, and liquid constituents are experimentally characterized, demonstrating materials which span four orders of magnitude in modulus and two orders of magnitude in toughness. By forming analytical mappings between relative concentrations of constituents at the microscale and resulting macroscale material properties, inverse material design is enabled; the method is showcased by printing artifacts with prescribed toughness and elasticity distributions. The properties of these composites are placed in the context of biological tissues, showing they have promise as mechanically plausible tissue mimics.

1. Introduction

In traditional mechanical design, the selection of suitable base materials has been likened to “choosing from a vast menu;” designers catalogue relevant properties (stiffness, toughness, density, conductivity, etc.) to inform these choices.^[1] By introducing voids to produce a foam, engineers can modify the microstructural geometry of these materials and profoundly influence the material properties, altering them by a factor of 1000 or more. However, like their base constituent materials, the material properties of these stochastic foams are not independently adjustable.^[2]

Composites extend the gamut of achievable material properties by combining two or more dissimilar constituent materials to achieve a favorable blend of properties.^[3] For example, combining concrete and steel rebar produces a composite with intermediate density, cost, and strength (relative to pure steel and pure concrete), while the natural composite nacre exhibits fracture toughness greater than each of its constituent materials.^[4,5] While many naturally-occurring composites (e.g., wood) exhibit material inhomogeneities and geometric features at the microscale, to-date most manufactured

engineering composite materials have been assembled at the macroscale.^[6]

Multimaterial additive manufacturing (AM) presents an opportunity to synthesize composite materials with desired mechanical properties in a fully automated fashion. These AM technologies control material distribution and geometric details at sub-100 μ m resolution.^[7] This has enabled exploration of composites with outstanding material properties (tough synthetic nacre, for example^[2,5,8]). Multimaterial AM also offers the ability to decouple a composite’s material properties and control them independently, which is unique among approaches discussed so far. In this work we prescribe the microscale distributions of rigid, elastomeric, and liquid base constituents and demonstrate continuous and independent control over

stiffness and toughness in composite materials fabricated via multimaterial inkjet 3D printing. This fundamentally inverts traditional material selection: instead of hunting for a suitable engineering material with the correct combination of material properties and crafting our design from that material, we specify a desired (and locally varying) set of material properties over a design and use AM to automatically fabricate it.

Numerous commercial vendors of multimaterial inkjet 3D printers exist, including Stratasys, 3D Systems, Mimaki, Keyence, Nanodimension, and Quantica. These systems operate in a similar manner, and employ arrays of multi-nozzle droplet generators to jet droplets of photopolymer materials that are subsequently bulk-polymerized by exposure to a UV source to form 3D objects.^[7] Two commercially available inkjet base materials (referred to as Agilus and Vero in the Stratasys ecosystem) have widely differing properties after photopolymerization, and can be combined in different ratios to yield composites. The first becomes a tough and flexible elastomer-type material and the second forms a rigid plastic; these will be referred to as the “elastomer” and “rigid” phases, respectively. These base materials are proprietary mixtures of acrylate, urethane acrylate, and epoxy acrylate monomers along with reactive diluents and viscosity modifiers. While a wide array of composite materials can be realized by combining these base materials at the microscale (**Figure 1A**), this design space remains largely uncharacterized, and nominal properties for only select few material combinations are available from manufacturers.

Composites composed of these elastomer and rigid base ingredients in fixed, manufacturer-determined ratios have been characterized in literature, showing an order of magnitude variation in shear modulus.^[9] This work is expanded by Meisel et al., who

L. T. Smith, R. B. MacCurdy
 Paul M. Rady Department of Mechanical Engineering
 University of Colorado Boulder
 1111 Engineering Dr. UCB 427, Boulder, CO 80309, USA
 E-mail: maccurdy@colorado.edu

 The ORCID identification number(s) for the author(s) of this article can be found under <https://doi.org/10.1002/adma.202308491>

DOI: 10.1002/adma.202308491

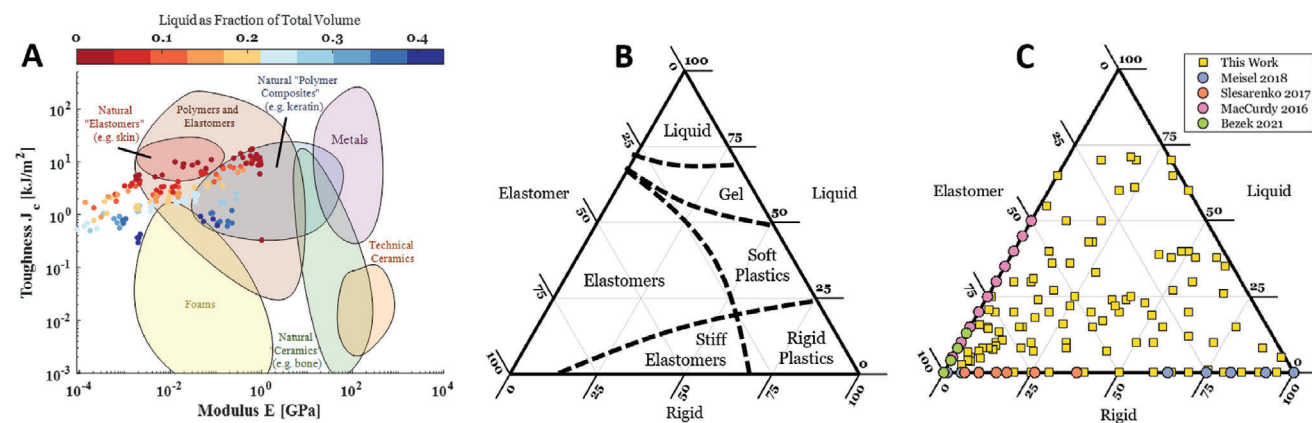


Figure 1. By controlling the concentrations of three base materials at the microscale via additive manufacturing, we realize composite materials with tunable mechanical properties that vary continuously across orders of magnitude (A) experimental results gathered in this paper are indicated, with color indicating the volume fraction fluid). These composites occupy a similar region of modulus-toughness space as biological materials (data in shaded regions from refs. [6] and [1]). B) Qualitative descriptors of resulting composite materials composed of rigid plastic, elastomeric, and liquid base materials vary widely. C) Previous efforts have restricted themselves to characterization of two-material composites only, appearing on the perimeter of the ternary axes. This work ventures off the perimeter of these axes, characterizing the richer design space of multiphase three-material composites at 110 positions in design space indicated by yellow squares.

formulate composites of random uniform mixtures of the same soft and rigid photopolymers, in different proportions than are offered by manufacturers.^[10] This unlocks an additional two orders of magnitude in storage modulus, as well as characterization of loss modulus across a wider range of mixing ratios. Mueller et al. quantify variations in elastic modulus and tensile strength as a function of build orientation and sample drying time in single-material specimens.^[7,11] Cazon obtains similar results for a different inkjet material,^[12] and Bass quantifies variations in material properties for homogeneous printed samples.^[13]

More recently, researchers have expanded the gamut of mechanical properties achievable in AM parts by modifying inkjet printing technology and introducing a non-curing liquids as build materials. This liquid is typically used in cleaning the resin lines of the printer and is a mixture of ethylene glycol and polyethylene glycol; it will be referred to as the “fluid” phase for the remainder of this work. MacCurdy et al. first used the technique to create multiphase composites with more highly tunable dissipative properties than stock inkjet materials.^[14] Bezek et al. repeated these measurements for a similar set of elastomer/fluid composites and expanded testing to quantify hardness, tensile behavior, and puncture response.^[15]

The extent to which these previous efforts have characterized the inkjet composites formulated from elastomer, rigid, and fluid phases is visualized on ternary axes in Figure 1C. Each point on these axes represents a unique mixture of three base materials in concentrations that can be read by following equilateral gridlines to the border of the axes. Critically, no previous efforts have characterized digital composites made up of three inkjet materials with widely differing profiles of mechanical properties: rigid plastic (e.g., Vero), soft elastomer (e.g., Agilus30), and liquids (e.g., ethylene glycol cleaning fluid). This is apparent in the distribution of circular dots of Figure 1C representing inkjet composites previously characterized in literature. These points lie strictly on the outer border of the axes, indicating they are two-material composites. In applications such as the creation of synthetic tis-

Table 1. Mechanical properties extracted from experimental testing, where F , σ_{11} , and ϵ_{11} represent uniaxial force, stress, and strain, respectively, ϵ_l and ϵ_f represent maximum strain in linear regime and fracture strain, respectively, R indicates indenter radius, δ represents indentation distance, and ν denotes Poisson’s ratio, assumed to be 0.5 throughout this work (appropriate for incompressible materials).

	Uniaxial tension	Spherical indentation
Elastic modulus (MPa)	$\sigma_{11}/\epsilon_{11} _{\epsilon_l}$	$\frac{3F(1-\nu^2)}{4R^{1/2}\delta^{3/2}}$
Elongation to fracture	$1 + \epsilon_f$	N/A
Toughness (J/m^3)	$\int_0^{\epsilon_f} \sigma_{11} d\epsilon_{11}$	N/A
Relaxation factor	$\max(F)/F_\infty$	$\max(F)/F_\infty$

sue mimics, where multiple mechanical properties (e.g., stiffness and toughness) must be simultaneously prescribed, these two-material composite fall short of mechanical realism.^[15,16]

In this work we “let go of the edge of the swimming pool,” and characterize the design space of novel three-material inkjet composites (Figure 1C). We demonstrate a method for repeatable fabrication of 3-material composites with prescribed material properties using inkjet additive manufacturing which, to our knowledge, has not been previously shown. We investigate quasistatic and time-varying material responses of these materials (notably elastic modulus, toughness, and elongation to fracture; see Table 1) in 188 tests on 110 unique composites and make these raw data available in Supporting Information and in a Github repository. We compare these properties to published data for a variety of tissues, showing that they span a wide range (up to four orders of magnitude) of biologically-relevant stiffness, toughness, and relaxation behaviors. We build data-driven mappings between the microscale concentrations of rigid, soft, and liquid component phases and macroscale material properties of the resulting composites, allowing the properties of composites not in our test set to be interpolated. We show through experimental observation, and validation via

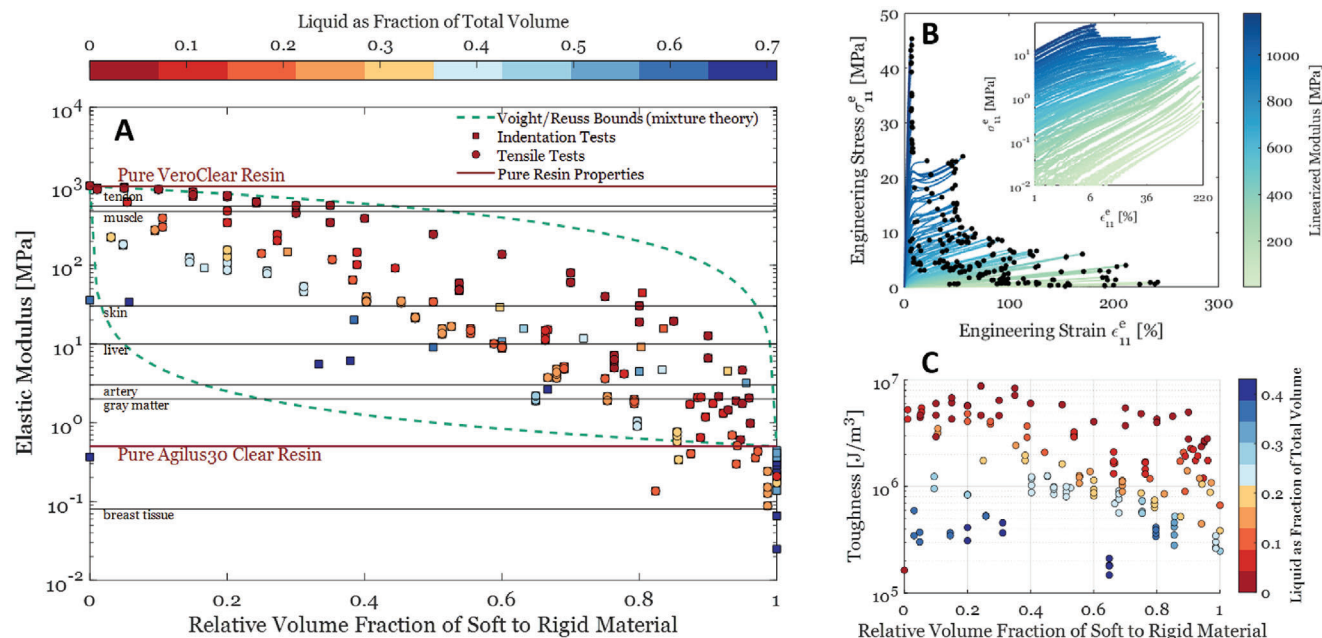


Figure 2. A) By structuring the distribution of multiphase constituents in inkjet composites, modulus values across four orders of magnitude are achieved. This range of stiffnesses spans a wide selection of biological tissues, with nominal values taken from literature.^[17] B) Examination of the stress-strain responses in uniaxial tension only reveals a tradeoff between elongation to break (sample fracture indicated by black points) and stiffness. Inset plot shows the same stress-strain data on logarithmic axes, highlighting the range of moduli and stress-strain responses exhibited by the composites tested here. C) Integration of stress-strain curves of B up to the point of failure yields a toughness measure, which varies over two orders of magnitude.

fabrication, that it is possible to prescribe mechanical properties like elastic modulus and toughness independently using just 3 base-materials in the composite system.

Finally, we demonstrate this by fabricating and characterizing an artifact with prescribed, locally varying stiffness and toughness properties. This example demonstrates our concept of “Pantone for properties”—just like deterministic color generation is possible using a small set of primary colors, our method enables deterministic control over mechanical properties using a small set of constituents. We note that while the experimental characterization presented in this work uses the photopolymer resins and printing system described elsewhere, there is nothing in our approach that is limited to these materials or any specific multi-material inkjet printing system.

2. Results

Elastic modulus values spanning four orders of magnitude are achieved in samples printed from varying concentrations of rigid, elastomer, and fluid phases combined in random distributions at the microscale. These stiffnesses range from ~ 20 kPa, comparable to the stiffness of fibroglandular tissues, to ~ 2 GPa, comparable to stiff tendon tissue.^[17] Figure 2A presents this elastic modulus for all composites tested in this work. Voigt/Reuss bounds are indicated in green; the lower bound is computed by excluding the elastic stiffness of the fluid constituent, which is assumed to be zero. Coloring of the dataset indicates the volume fraction of liquid in a given composite material, and the relative concentration of the remaining rigid and elastomer material is represented on the abscissa.

Many three-material composites with identical elastic stiffness and variable constitution are apparent (points which lie along horizontal lines in Figure 2A), a result that to our knowledge is not demonstrated in any previous investigation of two-material composites. The addition of liquid at a constant mixing ratio of solid (rigid/soft) constituents generally lowers the elastic modulus. Examination of the stress-strain responses in uniaxial tension only (Figure 2B) reveals a tradeoff between elongation to break (sample fracture indicated by black points) and stiffness.

These failure points in stress-strain space form an apparent envelope which bounds the maximum energy absorbed by a sample until failure. Integration under the stress-strain curves of Figure 2B up to the point of failure yields a toughness measure (Figure 2C) which varies over two orders of magnitude for the composites tested here. This toughness measure is plotted in a similar fashion to elastic modulus, and indicates that the addition of liquid to a constant mixing ratio of solid constituents strictly lowers the toughness. Critically, direct control over the mixing ratio of three base ingredients enables simultaneous and independent tailoring of stiffness and toughness, allowing for more complete matching to material property profiles found in biological tissues, for example. Historically, researchers have struggled to match the stiffness of biological tissues in synthetic analogues while simultaneously prescribing physically plausible toughness.^[18]

Stress relaxation tests indicate strong time-dependent elastic behavior in the composite materials tested here (a subset of these tests is given in Figure 3D), which is consistent with previous results.^[9,14,19] These tests are conducted via uniaxial tension ramp-hold tests described in Experimental Section, and we adopt

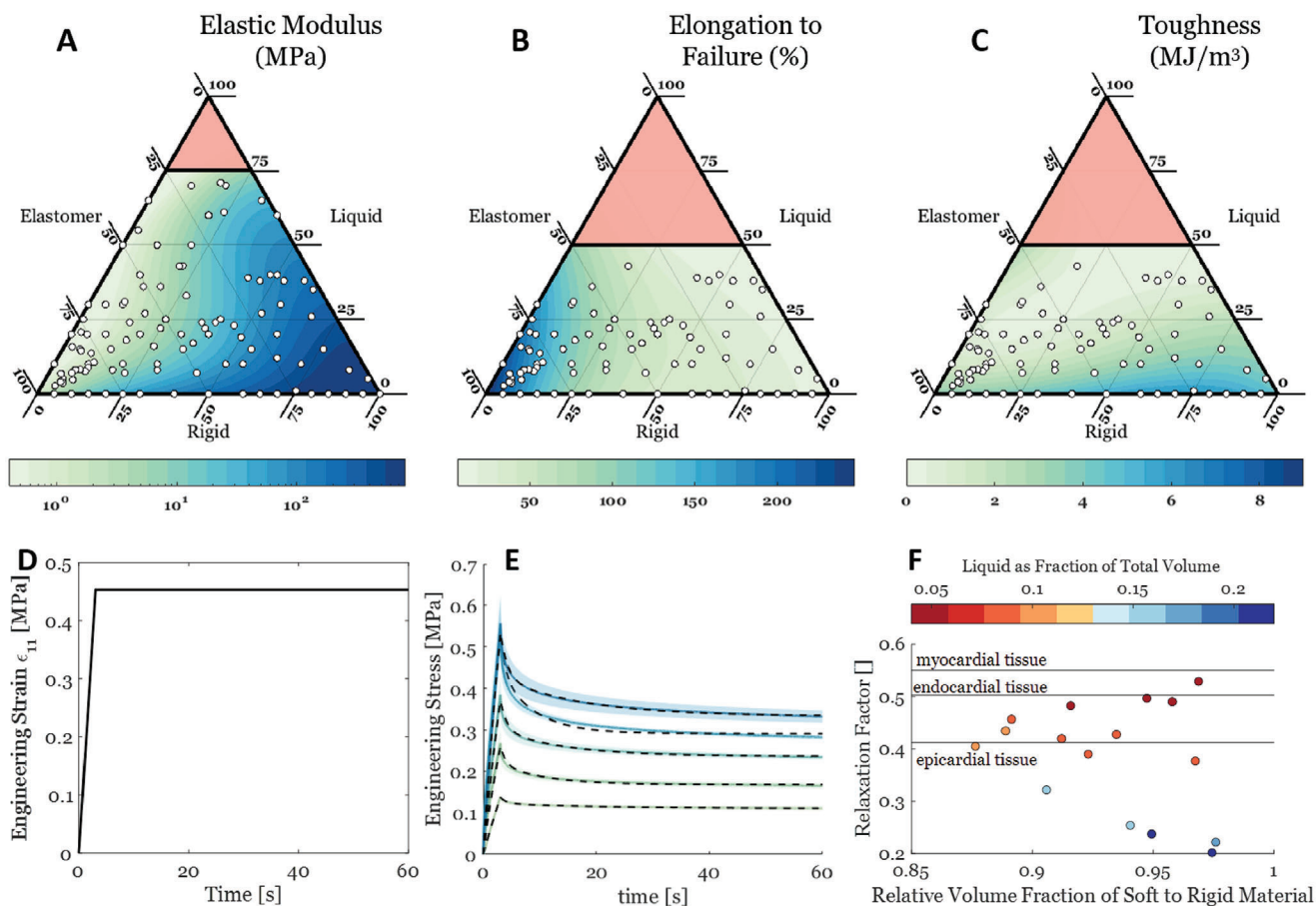


Figure 3. Mechanical properties measured in experimental testing of 188 unique multimaterial composites. A) Elastic modulus measured in uniaxial tension or spherical indentation and a corresponding analytical mapping. B,C) Elongation to failure and toughness respectively, both measured in uniaxial tension, along with analytical mappings. Analysis of fitting error and method of analytical model selection are detailed in [Supporting Information](#). Pink shaded areas on ternary plots indicate regions which were not feasible to test due to high liquid content (above 50% for uniaxial tension and above 75% for spherical indentation). D) A prescribed displacement ramp-hold test allows characterization of the time-dependent response of three-material composites, which exhibit a stress relaxation response. E) Results for five composites (indicated by different colors) are shown; shaded regions indicate 2σ variation from the mean of three tests. In order of increasing stress after relaxation, the composites are designated A76V02, A89V03, A84V07, A87V08, and A78V11 (using the format AxxVyy where xx indicates the percent composition elastomeric phase, yy indicates the percent composition rigid phase, and the remainder is fluid). F) Time dependent behavior is quantified by dividing the stress that has relaxed away at steady state into the peak stress, yielding a relaxation factor (RF) similar to cardiac tissue.^[18]

a relaxation factor (RF) metric similar to one previously used to characterize cardiac tissue.^[18] We define RF as the stress which relaxes away during the hold period of the test normalized by the peak stress (typically at the transition between the ramp and hold periods).

It is important to note that in this work we do not attempt to separate and quantify two conspiring mechanisms producing nonlinear time-dependent behavior which have been studied in biological tissues and biphasic composites: viscoelasticity and poroelasticity.^[20] Viscoelasticity refers to inherent rate-dependent behaviour of a material (even a homogeneous material), while poroelasticity refers to rate-dependent effects which arise from the deformation-driven flow of viscous fluid through a solid matrix (even a linear-elastic matrix). These mechanisms likely coexist for multiphase inkjet composites with sufficiently high liquid content; separating them would

require performing indentation testing with variable indentation rates and probe sizes, which is beyond the scope of this work.^[21]

Beyond simply characterizing multiphase digital materials, we enable inverse design of AM objects with prescribed properties by creating mappings between volume fraction of base materials at the microstructure and macroscale material properties. Analytical fits to the properties listed in [Table 1](#) are presented graphically on ternary axes in [Figure 3A–C](#). These fits take the form of polynomial surfaces represented by the equation below. We select the analytical form of these fit surfaces out of a desire for a compact, closed form predictive model. We select the polynomial order of each mapping by analyzing the standard error of the estimate (S_e) and the Akaike information criterion (AIC) as a function of increasing polynomial order; this latter measure permits comparisons between candidate models on the basis of accuracy

Table 2. Coefficients in analytical mappings between concentrations in base materials at the microscale, and macroscale material properties. Mappings take the form of Equation (1).

Property P	Fit Coefficients													
	a_{00}	a_{10}	a_{01}	a_{20}	a_{11}	a_{02}	a_{30}	a_{21}	a_{12}	a_{03}	a_{31}	a_{22}	a_{13}	a_{04}
log (modulus) MPa	-4.43	21.49	36.74	-36.95	-86.41	-82.73	19.93	41.8	125.6	86.39	25.97	-13.55	-60.33	-33.08
Elongation %	-83.88	307.9	221.6	180.8	-334.1	-136.0	-147.4	-640.7	222.8	0	0	0	0	0
Toughness MJ m ⁻³	-12.47	90.29	26.88	-165.6	-209.3	-9.963	91.45	214.2	139.4	0	0	0	0	0

and model complexity.^[22] Details are provided in Supporting Information.

$$P = a_{00} + a_{10}f_s + a_{01}f_r + a_{20}f_s^2 + a_{11}f_s f_r + a_{02}f_r^2 + a_{30}f_s^3 + a_{21}f_s^2 f_r + a_{12}f_s f_r^2 + a_{03}f_r^3 + a_{31}f_s^3 f_r + a_{22}f_s^2 f_r^2 + a_{13}f_s f_r^3 + a_{04}f_r^4 \quad (1)$$

where P indicates the property to be mapped, f_s indicates the volume fraction soft material and f_r indicates the volume fraction rigid material (the remaining fraction is liquid). Coefficients of these fits are listed in **Table 2**, enabling the estimation of mechanical properties for a variety of elastomer/rigid/liquid inkjet composites inside the design space indicated in **Figure 4A** (we do not recommend extrapolation outside this region). In this work we choose to define these mappings over the volume fraction of rigid plastic and elastomeric constituents; the concentration of liquid is fully defined by these two variables and does not appear in the fit equation. The polynomial degree of these surfaces was determined on a per-property basis to provide a compact analytical mapping between design space and material property space while minimizing fitting error.

The extrema of mechanical properties shown in **Figure 3** lie on the boundary of the convex hull around the experimental data in design space, which is indicated in **Figure 4A**. By computing three material properties (modulus, toughness, elongation to break) predicted by our analytical mappings inside this region, we can produce a constraint manifold in material property three-space (**Figure 4B**). In **Figure 4B**, black points represent experimental measurements, and the edges of the constraint manifold surface that correspond to the border of the design space in **A** is indicated in blue. The green surface itself in **Figure 4B** represents all points in material property space which are reachable by adjusting the mixing ratios of the three composite materials according to the method presented here. This constraint surface is contained in a bounding box that spans two orders of magnitude in elongation to break, one order of magnitude in toughness, and four orders of magnitude in elastic modulus.

Figure 4C–E show projections of the 3D constraint surface into subspaces formed by each unique combination of two material properties. This projection reveals closed areas where all unique combinations of mechanical properties presented in **Figure 3A–C** are simultaneously achievable, as predicted by

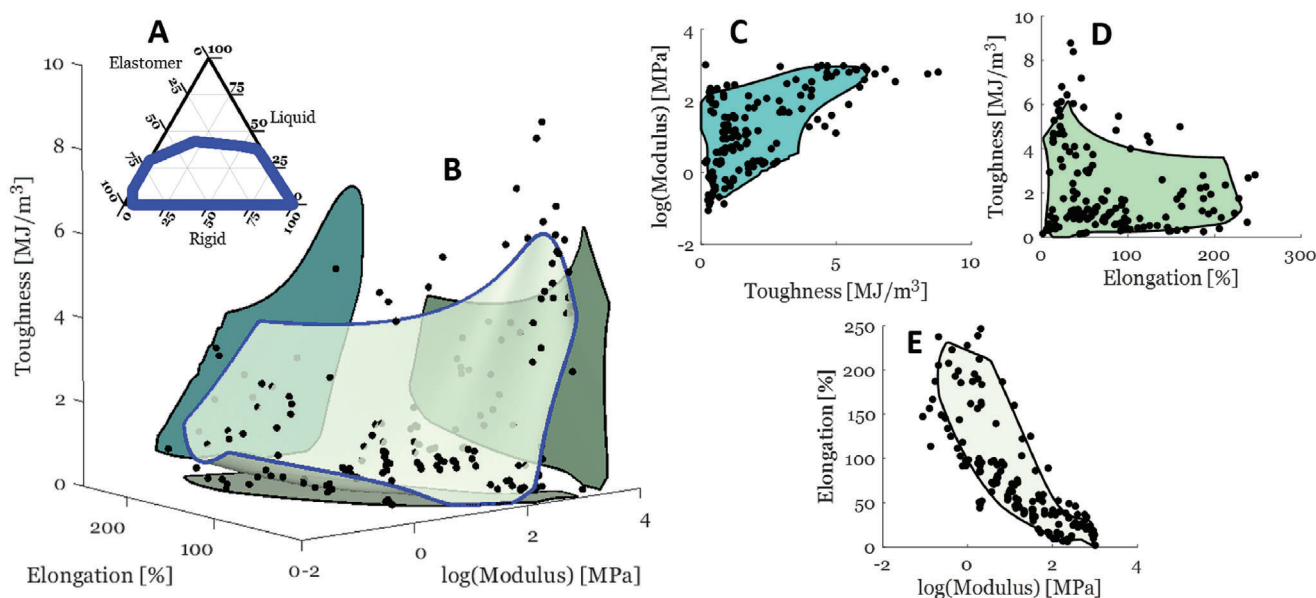


Figure 4. A) Regions of “simultaneously reachable material properties” can be defined by applying the mappings of **Table 2** to the region in design space indicated by the blue border (defining the limits of design space for which adequate experimental characterization is available). B) The constraint manifold indicates all possible material property tuples; C–E) projecting this manifold into material property two-space yields regions where any two of the three properties elastic modulus, elongation to fracture, and toughness can be independently prescribed. Black points indicate experimental measurements, and the shaded regions indicate reachable areas predicted by analytical mappings.

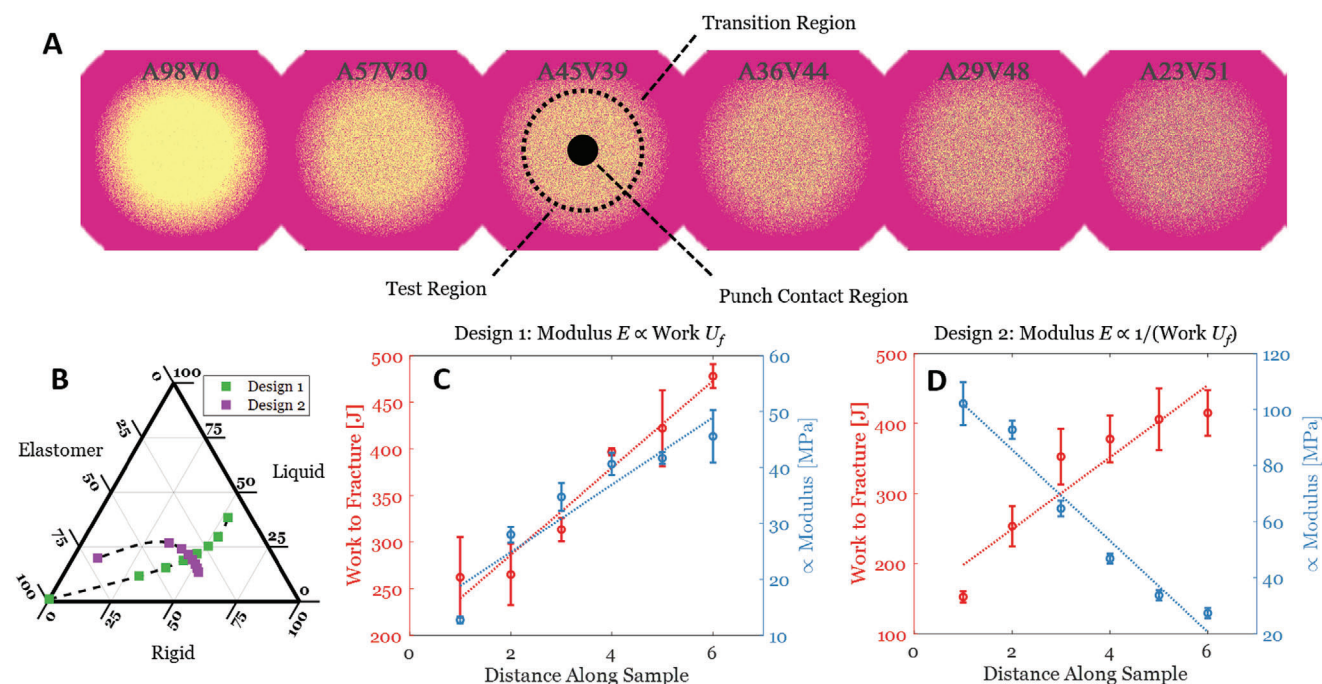


Figure 5. Demonstration of the degree of control over material properties that our approach offers designers. A) Test samples with prescribed stiffness and B–D) toughness distributions as a function of their length are designed using our method and characterized using a punch test, which allows us to infer the stiffness and measure the work to fracture of circular regions on the sample. The stiffness and work to fracture each vary linearly in proportion to each other in Design 1 (C; Design 1 pictured in (A)), and in inverse proportion in Design 2 (D), which demonstrates that the properties are independent and can be individually specified by our method. Trajectories through design space indicated in (B) are plotted through material property space in Supporting Information. Each sample is uniquely serialized according to the format described in the Experimental Section.

analytical mappings in Table 2. The size and shape of each region indicate the degree to which the associated two material properties are decoupled; inside these closed regions each property can be prescribed independently. Black datapoints in Figure 4C–E indicate that experimental measurements fall primarily inside the regions predicted by analytical mappings, though some outliers exist. Notably, the convex hulls around the experimental measurements (black points) in Figure 4C–E are superset of the boundaries predicted by analytical mappings in material property two-space, indicating a conservative model. High-resolution images of the constraint manifold in Figure 4B are given in Supporting Information, as well as a video file showing the manifold rotating in space.

This constraint surface in material property space (Figure 4B) can be used to perform inverse design of composite materials with multiple independently prescribed mechanical properties. To demonstrate the power of independent control over multiple material properties offered by this method, we fabricate two exemplar designs with prescribed, locally varying stiffness and toughness (Figure 5A). The distributions in each sample are chosen to demonstrate that the associated material properties are decoupled; experimental testing is used to interrogate these properties at regular intervals along the length of each sample.

In Design 1, we prescribe modulus and toughness to linearly increase along the length of the test sample, while in Design 2, we prescribe modulus to increase linearly and toughness to decrease linearly along the length. In order to determine the required relative concentrations of constituent materials to yield a specific

modulus/toughness combination (visualized as paths through ternary design space in Figure 5B, and through material property space in Supporting Information), we use a constrained nonlinear programming routine implemented in the Matlab function *fmincon()*. Constraints are defined to prevent the relative concentration of any material from falling below 0%, to limit the concentration of liquid to below 50%, and to enforce the condition that the sum of all concentrations be unity. When solving for sequential points in ternary design space which minimize error between prescribed material properties and the values predicted by the analytical mappings given in Table 2, we seed the nonlinear algorithm with the most recently solved point to improve convergence time. The implementation of this algorithm is freely available from <https://github.com/MacCurdyLab/DigitalMultiphaseMaterials>.

We mechanically characterize these designs by performing a punch test. Each bar is designed with a series of six circular test regions, surrounded by rigid material, with a graded transition region at the interface to reduce stress concentrations (Figure 5A). A stainless steel dowel is lowered through the punch region, indentation distance and force are recorded, and the test terminates when the material fails (indicated by a rapid loss of punch force). This test is devised to characterize the mixed-mode mechanical behavior of digital composites subjected to realistic loading conditions. We hypothesize that the integral under the force–displacement curve to the point of failure is linearly correlated to the toughness, and that the slope of the force displacement curve is proportional to the elastic modulus (this is an accepted

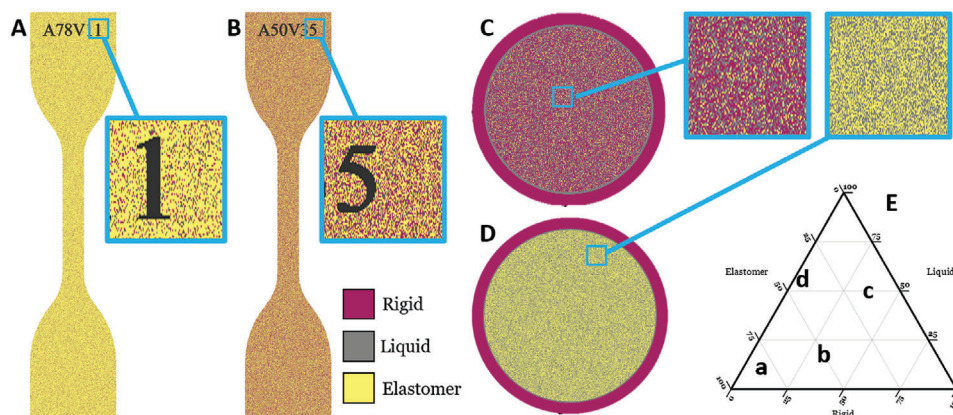


Figure 6. Samples are prepared for mechanical characterization via uniaxial tension or spherical indentation using in-house scripts that write stacks of bitmap images prescribing the distribution of print materials on a per-layer basis. A,B) Typical samples for uniaxial tension have lower levels of fluid concentration, and C,D) typical samples for spherical indentation have higher levels of liquid. E) The location in phase space of the four samples visualized here. Each sample is uniquely serialized according to the format described in the Experimental Section.

test method for linear elastic materials characterized in a “Small Punch Test”^[23].

Results indicate that these two measures of work-to-fracture and stiffness vary in proportion to each other in Design 1 (Figure 5C), and in inverse proportion to each other in Design 2 (Figure 5D). This suggests that the mappings presented in Table 2 may be used to infer changes in closely related material behaviors as a function of constitutive material concentration, and demonstrates the simultaneous and continuous control over two material properties in an additively manufactured multiphase composite. Critically, the test illustrates that the two properties are decoupled and can be specified independently.

3. Conclusion and Future Work

In this work we present the first characterization of the design space of three-material inkjet-3D-printed composites. We generate mappings between ratios of constituent materials at the microscale and macroscale material properties of the resulting composites. We investigate quasistatic and time-varying material responses and compare results to published data for a variety of tissues, showing that they span a wide range (up to four orders of magnitude) of stiffnesses, toughnesses, and relaxation behaviors. For the first time, we characterize a 3D region of material property space which is reachable by controlling the mixing ratios of rigid, elastomer, and liquid ingredients. Projections into lower-dimensional material property subspaces indicate that any two material properties may be decoupled using this approach. This decoupling is a direct consequence of the addition of a third base material into composite design space; a still-wider gamut of material properties would be reachable if arrangement of composite ingredients at the microscale were considered as a design variable. Finally, we demonstrate the inverse design and additive fabrication of a composite with multiple mechanical properties simultaneously prescribed, by leveraging the mappings developed during characterization.

In this work we focus entirely on homogenized material properties that arise from mixes between base ingredients in random uniform distributions. Previous work has shown that by directly

controlling the microstructure geometry of additively manufactured objects, wide variations in macroscale material properties can be achieved, even for solid/void cellular solids. Additionally, more in-depth testing on the time-varying elastic properties of multiphase inkjet composites could be performed to parse the impacts of base material viscoelasticity and composite poroelasticity for various concentrations of liquid to solid constituents.

4. Experimental Section

Characterization of mechanical properties for soft materials was multifaceted and may consist of tensile, indentation,^[17] bending, and harmonic excitation testing, as well as more applied characterization such as puncture,^[24] tear, fracture, and scratch.^[5] In this work, samples were characterized either by uniaxial tensile testing or spherical indentation testing depending on the volume fraction liquid; for liquid fractions above 50%, dogbones samples break down before reaching strain levels suggested by American Society for Testing and Materials (ASTM) D412C,^[25] necessitating indentation testing using disk-like samples. All samples were serialized during fabrication with a six-character code with the form $A_{xx}V_{yy}$, where xx indicates the percent composition elastomeric phase, yy indicates the percent composition rigid phase, and the remainder is fluid. Material properties extracted from experimental tests are listed in Table 1; more detailed explanations of experimental setups follow. Notably, local failure of material under test was not obvious in indentation testing; because toughness is typically computed as integrated energy up to failure this material property was not available from indentation testing. Fitting procedures are described in detail in Supporting Information, and raw data used for fitting is available for download <https://github.com/MacCurdyLab/DigitalMultiphaseMaterials>, allowing other practitioners to fit their own models to the data. Data were provided from 188 experimental tests on 110 unique three-material composite blends; 69 of these composites were tested once, 21 were tested twice, and 20 were tested three or more times.

Specimen Design: All test specimens were fabricated using a Stratasys J750 PolyJet system using the Voxel Print Utility. This utility allows users to directly control deposition of up to six different materials on a per-droplet basis throughout a volumetric print by sending sequential print layers to the J750 as bitmap images. In-house scripts were designed to generate bitmap stacks of specimen geometry according to mechanical test type. Samples were generated on a layer-by-layer basis, with appropriate masks used to create dogbone geometry (e.g., Figure 6A,B), cylindrical shapes, and lettering for serialization (to apply sample ID labels), as well as

account for the nonuniform print resolution of the printing hardware used in this work (600 × 300 dpi in the XY plane with a layer height of 27 μm). In the case of indentation samples (e.g., Figure 6C,D) a rigid polymer cup was printed around the cylindrical sample to prevent liquid migration.

Test regions of all samples had spatially independent, random uniform distributions of the three base materials in prescribed proportions according to the location in ternary design space shown in Figure 1. As samples were generated, the as-designed ratios of constituent materials were monitored to ensure they remain within 0.1% of prescribed design proportions. Position in constituent material space for the example specimens pictured in Figure 6 are given in Figure 6E; the locations in three-material design space were chosen at random using a Latin hypercube method. Scripts used to create print files for test samples generate each layer of each sample (even replicate samples) as a unique, uniform random distribution of materials in these specified proportions, ensuring that homogenized material properties can be extracted from macroscale experimental tests. Meisel et al. have quantified the length scale separation (~20 ×, or 2 mm at J750 print resolution) between build resolution and feature size above which random microstructure variation played a minimal role in macroscale property uncertainty.^[10] Following these results, all dogbone samples were fabricated with a minimum thickness of 2 mm, a spherical probe with 2.5 mm radius R was used for indentation testing, and a steel pin with 2.5 mm radius was used for punch testing. Indentation samples were fabricated with a test region radius $5 \times$ larger than the probe radius R and a height $5 \times$ taller than the max probe depth δ , mitigating the impacts of edge effects.

Mechanical Characterization—Uniaxial Tension: A low-force, high-stroke load frame (dynamic material analyzer, or DMA) was used for all mechanical characterization (810E5 All-Electric Dynamic Test Machine, Test Resources), which had a position accuracy of ± 0.1 μm and a force measurement accuracy of ± 0.4 N. Tensile test specimens were designed and tested according to ASTM standard D412 (Die C, 33 × 6 × 2.0 mm³ test region), Test Methods for Vulcanized Rubber and Thermoplastic Elastomers - Tension.^[25] This standard details a methodology for determining the proper strainrate $\dot{\epsilon}$ at which to test rubber dogbone samples, which varies according to the stiffness of the sample under test. By following this methodology all samples were tested at constant strainrates of $\dot{\epsilon} \in (0.01, 0.25)$ (crosshead velocity $v \in (25, 500)$ mm/min⁻¹) up to ultimate failure of the sample. In post-processing, the as-tested strainrate was computed by numerically differentiating the displacement. Similarly, in post-processing the stress and strain were zeroed by a digital trigger on the DMA's output force signal, with the trigger level set to 1% of the peak force in the test.

Additional ramp-hold tensile testing was performed on a selection of composite materials with varying levels of viscoelastic characteristics. In these tests, samples were drawn in uniaxial tension to an engineering strain ϵ of 0.45, at constant strainrate $\dot{\epsilon}$ of 0.1 s⁻¹ then held at constant strain for 100 s. Table 1 gives the mechanical properties computed from uniaxial tensile tests, which include secant elastic modulus (computed at the maximum strain in linear regime, ~1–4 ultimate strain), elongation to fracture, toughness, and relaxation factor (in the case of ramp-hold tests).

Mechanical Characterization—Spherical Indentation: The same DMA was utilized for indentation testing, with a custom spherical probe attachment fabricated from stainless steel. An indenter with radius $R = 2.5$ mm was used to contact the center of cylindrical indentation samples, with alignment in the horizontal plane achieved by a custom AM jig. All samples were tested at a constant indentation velocity of 10 mm/min⁻¹ up to an indentation distance $\delta = 2R$. Similar to tensile testing, in post-processing the start of the test was triggered on the DMA's output force signal, with the trigger level set to 1% of the peak force in the test.

Supporting Information

Supporting Information is available from the Wiley Online Library or from the author.

Acknowledgements

This research is supported by the University of Colorado through a research grant awarded by the Anschutz-Boulder Nexus Initiative, by a Sandia National Laboratories matching grant (AWD-23-03-0079), and by internal MACLab startup funds at the University of Colorado, Boulder.

Conflict of Interest

The authors declare no conflict of interest.

Data Availability Statement

Experimental data presented in this work, analytical mappings between composite microstructure and macroscale materials properties, and custom code for inverse material design are freely available from <https://github.com/MacCurdyLab/DigitalMultiphaseMaterials>.

Keywords

additive manufacturing, digital composites, material characterization, multiphase materials

Received: August 21, 2023

Revised: December 20, 2023

Published online:

- [1] M. F. Ashby, *Materials Selection in Mechanical Design*, Vol. 16, Elsevier, New York 2014.
- [2] M. F. Ashby, *Philos. Trans. R. Soc. A: Math., Phys. Eng. Sci.* **2006**, 364, 15.
- [3] G. W. Milton, *The Theory of Composites*, SIAM, Philadelphia, PA 2002.
- [4] M. M. Porter, J. Mckittrick, S. Diego, *Am. Ceram. Soc. Bull.* **2015**, 93, 18.
- [5] J. W. Pro, F. Barthelat, *MRS Bull.* **2019**, 44, 46.
- [6] U. G. K. Wegst, M. F. Ashby, *Philos. Mag.* **2004**, 6435, 2004.
- [7] J. Mueller, K. Shea, C. Daraio, *Mater. Des.* **2015**, 86, 902.
- [8] M. J. Mirzaali, M. Cruz Saldivar, A. Herranz de la Nava, D. Gunashekar, M. Nouri-Goushki, E. L. Doubrovski, A. A. Zadpoor, *Adv. Eng. Mater.* **2020**, 22, 7.
- [9] V. Slesarenko, S. Rudykh, *Soft Matter* **2016**, 12, 3677.
- [10] N. A. Meisel, D. A. Dillard, C. B. Williams, *Rapid Prototyping J.* **2018**, 24, 872.
- [11] J. Mueller, S. E. Kim, K. Shea, C. Daraio, in *Proc. of the ASME Design Engineering Technical Conf.* ASME, New York **2015**, pp. 1–10.
- [12] A. Cazón, P. Morer, L. Matey, *Proc. Inst. Mech. Eng., Part B* **2014**, 228, 1664.
- [13] L. B. Bass, N. A. Meisel, C. B. Williams, in *Proceedings - 26th Annual International Solid Freeform Fabrication Symposium - An Additive Manufacturing Conference, SFF 2015*, The Minerals, Metals & Materials Society, Pittsburgh, PA **2020**, pp. 993–1006.
- [14] R. MacCurdy, J. Lipton, S. Li, D. Rus, in *IEEE Int. Conf. on Intelligent Robots and Systems*, IEEE, Piscataway, NJ **2016**, pp. 2628–2635.
- [15] L. B. Bezek, C. A. Chatham, D. A. Dillard, C. B. Williams, *J. Mech. Behav. Biomed. Mater.* **2021**, 125, 104938.
- [16] R. Ratnam, M. Quayle, J. Crock, M. Lazarus, Q. Fogg, P. McMenamin, *J. Anat.* **2019**, 234, 419.
- [17] C. T. McKee, J. A. Last, P. Russell, C. J. Murphy, *Tissue Eng. - Part B: Rev.* **2011**, 17, 155.
- [18] H. Riedle, P. Molz, J. Franke, in *2018 IEEE EMBS Conf. on Biomedical Engineering and Sciences, IECBES 2018 - Proc.*, IEEE, Piscataway, NJ **2019**, pp. 171–176.

- [19] D. Blanco, P. Fernandez, A. Noriega, *J. Mater. Res.* **2014**, *29*, 1876.
- [20] R. A. Regueiro, B. Zhang, S. L. Wozniak, *Comput. Model. Eng. Sci.* **2014**, *98*, 1.
- [21] M. Galli, K. S. Comley, T. A. Shean, M. L. Oyen, *J. Mater. Res.* **2009**, *24*, 973.
- [22] L. Marechal, P. Bolland, L. Lindenroth, F. Petrou, C. Kontovounisios, F. Bello, *Soft Rob.* **2021**, *8*, 284.
- [23] E. Lucon, J. T. Benzing, N. Derimow, N. Hrabe, *J. Mater. Eng. Perform.* **2021**, *30*, 5039.
- [24] B. Esterer, M. Hollensteiner, A. Schrempf, M. Winkler, S. Gabauer, D. Fürst, R. Merwa, S. Panzer, K. Püschel, P. Augat, *J. Mech. Behav. Biomed. Mater.* **2020**, *110*, 103946.
- [25] J. W. Gooch, *ASTM D412-15 Standard Test Methods for Vulcanized Rubber and Thermoplastic Elastomers*, ASTM, Washington, D.C. **2011**.